The EP3–ZNF488 Axis Promotes Self-Renewal of Glioma Stem-like Cells to Induce Resistance to Tumor Treating Fields

Dongjiang Chen[1, #], Son B. Le[1, #], Harshit Manektalia[1], Tianyi Liu[1], Tarun E. Hutchinson[2], Adam O'Dell[1], Bodour Salhia[3, 4], and David D. Tran[1, 4, *]

[1] Division of Neuro-Oncology, Brain Tumor Center, Keck School of Medicine of University of Southern California, Los Angeles, CA 90033

[2] Department of Pediatrics, College of Medicine, University of Florida, Gainesville, FL 32611

[3] Department of Translational Genomics, Keck School of Medicine of University of Southern California, Los Angeles, CA 90033

[4] USC Norris Comprehensive Cancer Center, Keck Medicine of USC, Los Angeles, CA 90033

[#] These authors contributed equally to this work.

Running Title: The EP3–ZNF488 axis regulates GSC and TTFields resistance

[*] Corresponding author:

David D. Tran

Norris Comprehensive Cancer Center of USC

Harlyne J. Norris Cancer Research Tower (NRT) #7505

1450 Biggy Street, Los Angeles, CA 90033

david.tran@med.usc.edu

Conflict of interest: D.D.T. has received research grants, personal honoraria and the Inovitro™ system from Novocure to support parts of the work reported in this manuscript. However, the conceptualization, design, data collection, analysis, interpretation, decision to publish, and manuscript preparation were performed by the authors independently of Novocure. D.C., S.B.L., and D.D.T. are inventors of 1 patent application (62/849,535) based on some of the data in this manuscript. However, commercialization rights were transferred to Novocure per the funding agreement. D.D.T. has also received research funding from Merck, Sarepta, Novartis, Northwest Biotech, Monteris, and Lacerta for other unrelated work. All other co-authors declare no competing interests.

Abstract

Tumor Treating Fields (TTFields) employ low intensity, alternating electric fields to exert antitumor activity and have demonstrated efficacy against multiple cancers, including glioblastoma (GBM). Unfortunately, cancer cells inevitably develop resistance to TTFields, highlighting the need to elucidate the underlying mechanisms to develop approaches to induce durable responses. Using a gene network-based machine-learning algorithm, we interrogated TTFields-resistant GBM cells and uncovered a regulatory axis anchored by the prostaglandin E receptor 3 (EP3) and the transcription factor zinc finger 488 (ZNF488). Mechanistically, TTFields induced EP3 upregulation and nuclear envelope localization, where it formed a complex with ZNF488 to induce resistance to TTFields by promoting self-renewal of glioma

stem-like cells (GSC). Overexpression of EP3 and/or ZNF488 in TTFields-sensitive GSC conferred resistance and enhanced self-renewal, while expression of non-interacting mutants of these proteins abrogated formation of the nuclear complex and prevented resistance. Inhibition of either partner in this protein complex in resistant GSC, including those freshly isolated from TTFields-resistant GBM tumors, re-sensitized cells to the cytotoxic effects of TTFields, concomitant with reduced self-renewal and *in vivo* tumorigenicity. Importantly, inhibition of EP3 in TTFields-sensitive GSC preemptively halted the development of resistance. The EP3–ZNF488 axis was significantly upregulated in TTFields-resistant GBM tumors, and co-expression of EP3 and ZNF488 in other cancers correlated with lower survival rates. Collectively, these results indicate that the nuclear EP3–ZNF488 axis is necessary and sufficient to establish TTFields resistance, underscoring the potential to target this axis to prevent or reverse resistance in GBM and possibly other cancers.

Significance: The EP3–ZNF488 master regulatory axis in cancer stem-like cells drives resistance to treatments like tumor treating fields, opening avenues for developing strategies to enhance therapeutic efficacy.

Introduction

TTFields therapy is approved for glioblastoma (GBM) (1) and pleural mesothelioma (2), and is in advanced clinical trials for lung (3), pancreatic, hepatocellular carcinomas, and brain

3

metastasis. TTFields employ non-invasive, low intensity, alternating electric fields to exert antitumor effects through various cellular and molecular mechanisms. These include chromosome mis-segregation, breakage, and incomplete cytoplasmic separation, leading to mitotic catastrophe and p53-dependent or -independent apoptosis (4, 5). TTFields also disrupt DNA repair mechanisms, cause replication stress (6, 7), promote autophagy (8), and increase plasma membrane permeability, especially in tumor cells, leading to membrane-damage cell death (9). Recently, TTFields were shown to cause focal rupture of the nuclear envelope during the S phase of the cell cycle, releasing large DNA clusters into the cytosol, which activates DNA sensors inflammasomes (e.g., cGAS/STING and AIM2/Caspase-1). This targeted activation produces proinflammatory cytokines, type 1 interferons (T1IFN), and induces immunogenic cell death, releasing tumor antigens, and providing a multi-dimensional tumor immunizing platform (10). In a Phase 3 randomized study (1), TTFields plus chemotherapy significantly improved progression-free survival in newly diagnosed GBM patients (from 4 to 6.7 months). However, resistance to TTFields eventually develops, leading to treatment failure and disease progression. The molecular mechanisms of TTFields resistance are not well understood, underscoring the need for new therapeutic strategies to reverse resistance and enhance patient outcomes.

Previous experimental and computational models suggested that the optimal TTFields frequency is positively correlated with cytoplasmic conductivity and membrane thickness — the cell's dielectric properties — and inversely correlated with cell size (11-13). Tumor cells often increase in size in response to TTFields, possibly due to TTFields-induced plasma membrane compromise (9), suggesting a plausible mechanism for TTFields resistance (14, 15). However, this concept has not been validated in bona fide TTFields-resistant cells. Resistance might involve altering dielectric properties or restructuring biological pathways induced by the physical

forces, or both. In this study, we used an advanced machine-learning algorithm combined with rigorous experimental validation to delineate a novel regulatory subnetwork underlying TTFields resistance. This subnetwork is orchestrated by a partnership between prostaglandin E2 receptor 3 (PTGER3 or EP3), a seven-transmembrane G protein-coupled receptor (GPCR), and zinc finger 488 (ZNF488), a member of the highly conserved C2H2-type zinc finger transcription factor family. EP3 has diverse biological and pathological effects, including smooth muscle contraction (16), platelet aggregation (17), inflammation (18), and tumor growth and metastasis (19). ZNF488 plays essential roles in CNS development and differentiation (20, 21). Dysregulation of EP3 or ZNF488 has been linked to poor outcomes in various malignancies (22-25). We demonstrate that EP3 localizes to the nuclear envelope in GBM cells under TTFields treatment, where it binds nuclear ZNF488. The EP3–ZNF488 axis forms a tightly regulated epistatic complex that promotes TTFields resistance by enhancing self-renewal and *in vivo* tumorigenicity of GSC. This complex provides a novel insight into the mechanisms of TTFields resistance, offering potential targets for therapeutic intervention to overcome resistance and extend survival.

Materials and Methods

Antibodies

For immunofluorescence and immunoblotting: Primary antibodies — LaminAC (Santa Cruz, Cat#sc-7292, RRID:AB_627875 and 376248-AF488, RRID:AB_10991536), EP3 (Santa Cruz, Cat#sc-57105, RRID:AB_630173; Proteintech, Cat#14357-1-AP, RRID:AB_2237964), ZNF488 (DSHB, Cat#PCRP-ZNF488-1A6, RRID:AB_2619413; Invitrogen, Cat#PA5-98263,

RRID:AB_2812876), α-tubulin (Thermo Fisher Scientific, Cat#A11126, RRID:AB_10563441), 6xHis (Invitrogen, Cat#MA1-21315, RRID:AB_557403), Flag (Invitrogen, Cat#PA1-984B, RRID:AB_347227), and β-actin (Santa Cruz, Cat#sc-47778, RRID:AB_626632). Secondary antibodies — goat anti-mouse-A555 (Jackson Immunoresearch, Cat#111-295-003, RRID:AB_2338022); goat anti-rabbit IgG-A647 (Jackson Immunoresearch, Cat#111-605-003, RRID:AB_2338072); HRP-conjugated anti-mouse (Santa Cruz, Cat#sc-516102, RRID:AB_2687626); HRP-conjugated anti-rabbit (Enzo, Cat#ADI-SAB-300-J, RRID:AB_11179983); IRDye 680RD anti-Rabbit IgG Secondary Antibody (LI-COR, Cat#926-68071, RRID:AB_10956166); and IRDye 800CW anti-Mouse IgG Secondary Antibody (LI-COR, Cat#926-32210, RRID:AB_621842). Flow cytometry antibodies: ALDH1A1 (BioLegend, Cat#861902, RRID:AB_2801236) and CD133 (BioLegend, Cat#372806, RRID:AB_2632882).

Bulk RNA sequencing (RNA-seq)

RNA was extracted utilizing QIAGEN RNeasy Midi Kit (Cat#75144) according to the manufacturer's instructions for both *in vitro* cultured cells and snap frozen tumor tissues. Bulk RNA-seq library was constructed, pooled, and sequenced on a NovaSeq 6000 Illumina instrument (RRID:SCR_016387). Paired-end reads were trimmed with trimmomatic v/0.36 (RRID:SCR_011848), and alignment and gene counts generated against the GRCh38.p12 genome assembly using the annotation GeneCode release 28 by STAR v2.6.0b (RRID:SCR_004463) with default options and quantmode=GeneCounts.

Generation of lentiviral expression constructs for viral production

ORF expression clones for and human EP3 and ZNF488 were purchased from Genecopoeia (RRID:SCR_003145), and sequence verified. The backbones for overexpression and knock-down are LV120 and pLL3.7 (RRID:Addgene_11795), respectively. The truncated EP3 and ZNF488 overexpression plasmids were made by GenScript (RRID:SCR_002891) with the backbone pGenLenti. The deleted sequences are EP3-N: AACCACTCCTACACAGGCATGTGGGCGCCCGAGCGTTCCGCCGAGGCGCGGGGC; EP3-IL2: GAGCGGGCGCTGGCCATCAGGGCGCCGCACTGGTATGCGAGCCACATGA AGACGCGTGCCACCCGC; EP3-C: AGAAAGATCCTTCTTCGAAAGTTTTGCCAGGTAG CAAATGCTGTCTCCAGCTGCTCTAATGATGGACAGAAAGGGCAGCCTATCTCATTAT CTAATGAAATAATACAGACAGAAGCA; ZNF488-RD: GCGGAGCTGGCACTGTTGGTA GCCCCAGGCAAGCCCCGACCTGGCAAGCCGCTGCCCCCGAAGACACGTGGAGAGCA GAGGCAGAGCGCCTTCACGGAGCTGCCGAGGATGAAGGACCGGCAGGTGGATGCTC AGGCCCAGGAGAGGGAGCACGATGACCCCACAGGCCAACCTGGTGCCCCACAGCTG ACCCAGAACATCCCCAGAGGCCCAGCTGGCAGCAAAGTCTTCTCTGTGTGGCCCAG CGGAGCACGAAGTGAGCAAAGAAGCGCCTTTAGCAAACCAACCAAGCGACCAGCA GAGAGGCCTGAGCTAACCTCAGTCTTCCCTGCAGGGGAATCTGCAGAT; ZNF488-ZF: TGTGCAAAGTGCAACCTGTCCTTTCGCCTAACGTCCGACCTGGTCTTTCACATGCGAT CCCAC. For lentiviral production, 7.5×10^6 HEK 293T cells were plated overnight in intact DMEM in a 10cm Poly-D lysine hydrobromide (SIGMA) coated dish, followed by transfection with a 3:1 ratio of total DNA in PEI (µg) together with the viral packaging and envelop plasmids PSPAX2 (RRID:Addgene_12260) and PMD2.G (RRID:Addgene_12259), respectively in advanced DMEM medium supplemented with 1.25%FBS, 1X pyruvate, 10mM HEPES and 10mM sodium butyrate. Media were replaced at 16 hrs. after transfection. Viral supernatants

were collected every 24hrs and centrifuged for 20hrs. at 25,000g to sediment viral particles, which were resuspended in opti-MEM and viral titers measured.

Cell Culture

The patient-derived GSC lines CA3, CA7, and L2 [generous gift from Brent Reynolds, 2016-2018, previously characterized in (26, 27)], and GSC23, GSC33, and GSC122 (generated from TTFields-resistant GBM tumors according to an IRB-approved protocol, 2020-2022) were grown in stem cell media (STEMCELL, Cat#05750 with bFGF, EGF and heparin). Human GBM cells U87MG (ATTC, RRID:CVCL_0022; 2020) (28), LN428 (RRID:CVCL_3959) and LN827 (RRID:CVCL_6843) (26) (generous gifts from Joshua Rubin in 2015), MDA-MB-231 (ATCC, RRID:CVCL_0062; 2020), A549 (ATCC, RRID:CVCL_0023; 2020), and PANC-1 (ATTC, RRID:CVCL_0480), Hela (a generous gift from Brain K. Law, RRID:CVCL_0030; 2024), UMUC-3 (a generous gift from Amir Goldkorn, RRID:CVCL_1783; 2024), B16 (a generous gift from Bingfei Yu, RRID:CVCL_F936; 2024) were grown in DMEM media supplemented with 10% FBS and 1% pen/strep. The other lines T24 (a generous gift from Amir Goldkorn, RRID:CVCL_0554; 2024) and 786-O (a generous gift from Alan Epstein, RRID:CVCL_1051; 2024) were cultured in RIPA 1640 media supplemented with 10% FBS and 1% pen/strep. Cells were used for experiments within 7 days of thawing or no more than 2-3 passages dependent on the cell line, except for during the generation of resistant cells. Cells were authenticated by the short tandem repeats (STR) method on a representative aliquot with the most recent performed in 2022. Mycoplasma screen was performed yearly. TTFields were applied to cancer cell lines using the Inovitro™ system (Novocure, Israel). GBM cells were treated with TTFields at the clinically approved frequency of 200 kHz while the other cancer lines were treated at the

frequency of 150 kHz. Temozolomide was used at the concentration of 100μM. All chemical agents used in the study were purchased from Sigma except for the EP3 inhibitors L798,106 and DG041, which were purchased from Tocris.

Live cell imaging and enumeration

Adherent cells were harvested using 0.25% Trypsin, rinsed, and resuspended in DPBS. The number of live cells was determined using the TC20 Automated Cell Counter from BioRad, using Trypan Blue. For the stemness assay, live cells were resuspended in stem cell media, re-seeded into 96-well plates, and incubated for up to 2 weeks. Plates were then briefly centrifuged to settle cells at the well bottoms. To quantify live cells, the Invitrogen™ Calcein AM, a cell-permeant dye was used, following the manufacturer's instructions. Fluorescent and bright-field images of the cells were captured using a Molecular Device SpectraMax i3x microplate reader or ImageXpress Pico Automated Cell Imaging System. Sphere number and area were quantified using SoftMax Pro Software (RRID:SCR_014240) or ImageJ (RRID:SCR_003070).

Extreme limiting dilution assay (ELDA)

Cells were plated at 5-fold serial dilution from 3000 to 1 cell per well in non-adhering 96-well plates (Corning). The number of wells with visible spheres were enumerated 14 days later and percent sphere-forming cell frequency calculated using the ELDA software (RRID:SCR_018933) (29).

Immunofluorescence and Confocal Microscopy

Cells grown on cover slips were fixed with 4% paraformaldehyde for 30 min at 4°C, permeabilized with 0.1% cold Triton X-100 in PBS for 15 min at 4°C, blocked with 5% normal goat serum in PBS for 1 hr at 4°C, and incubated overnight at 4°C with different combinations of primary antibodies (dilution 1:500) against indicated antigens and then for 2 hrs at room temperature with appropriate fluorochrome-conjugated secondary antibodies (dilution 1:500). Labeled cells were counterstained with DAPI (Thermo Fisher, Cat#D1306, RRID:AB_2629482) at 1µg/ml for DNA content, and images captured and analyzed using a Zeiss 800 inverted confocal microscope. Images were captured at 63X oil immersion objective either at 0.5X or 1X zoom, keeping all the conditions of microscope, exposure, and software settings identical for all samples. The Z-stack analysis was performed by obtaining 15 to 20 (1µm thickness each) optical sections for each microscopic field. The Arivis software was used to generate 3D microscopy image and to observe 360° panoramic view of microscopy field. For all other analyses, Zen software (RRID:SCR_013672) was used.

Quantitative RT-PCR

QIAGEN RNeasy Mini Kit (Cat#74106) was used to extract RNA from cells/tissues according to the manufacturer's protocol. One µg total RNA was subjected to reverse transcription using iScript cDNA Synthesis Kit (BIO-RAD, Cat#1708891). qPCR was performed using Luna Universal qPCR Master Mix (NEB, Cat#M3003E) and on Bio-Rad CFX96 qPCR/RT PCR w. C1000 Touch Base (RRID:SCR_018064). Primers used are as follow: hEP3 forward (fw) CACACACGGAGAAGCAGAAA, reverse (rev) ACAGCAGGTAAACCCAAGGA; hZNF488

10

fw TAGCAAACCAACCAAGCGAC, rev GTTGAGGAGTCCAGACAGCT; hGAPDH fw GGCATGGACTGTGGTCATGA, rev ACCACCATGGAGAAGGC; hETV4 fw GATGATGTCTGCGTTGTCCC, rev AGCAAGGCCACCAGAAATTG; hTGFA fw CGCTCTGGGTATTGTGTTGG, rev TGGGAATCTGGGCAGTCATT; hDAAM2 fw CCTCACTCATTGGCTGCATC, rev GGTCTTGCTGTTCTCTGTGC; hEDA fw GGAACTCGAGAAAACCAGCC, rev ACCAGTCATTGAGCACTCCA; hHR fw GCCATCTCAAGAGTGACCCT, rev CAGGCCAGACACTAGGTAGG; hFCRLA fw GTCAGACAAAGTTGCCCCTG, rev TCTGAAGCTGTGGGGATCTG; hATP8A1 fw TCTTCGAGGAGCTCAGTTGA, rev TCAGCTTGGTGTCATGTCCA.

Immunoblotting and immunoprecipitation

Cells were treated for 20 minutes on ice with RIPA buffer (150mM NaCl, 1% NP-40, 0.5% Sodium deoxycholate, 0.1% SDS, 25mM Tris with a pH of 7.4) containing a protease inhibitor cocktail from Roche, followed by centrifugation at 13,000g at 4°C for 20 minutes. Total protein of collected supernatants was quantified using a protein assay dye kit (Bio-Rad). For subcellular fractionation, the Subcellular Protein Fractionation Kit for Cultured Cells by Thermo Scientific (Cat#78840) was employed. Equal amounts of total lysates were resolved by SDS-PAGE, transferred to PVDF membranes, which were blocked with 5% Bovine Serum Albumin (BSA) in Tris-Buffered Saline (TBS). Blocked membranes were then probed with specific primary antibodies at a 1:1000 ratio at 4°C overnight, rinsed with TBST, probed with species-specific HRP- or fluorescence-conjugated secondary antibodies at a 1: (1000-2500) dilution at room temperature for an hour, and quantified using the BIO-RAD ChemiDoc (RRID:SCR_019037) or the LI-COR Odyssey DLx (RRID:SCR_014579), respectively. For the immunoprecipitation,

11

equal amounts of total lysate input from cells were incubated with PTGER3 (ProteinTech, Cat#14357-1-AP), 6xHis, Flag antibody or the IgG1 control (R&D, Cat# AB-105-C, RRID:AB_354266), IgG2B (R&D, Cat# MAB004, RRID:AB_357346) using the Pierce™ Classic Magnetic IP/Co-IP Kit (Thermo, Cat#88804). Immune complexes were resolved by SDS-PAGE and subjected to immunoblotting for 6xHis, Flag, EP3 and ZNF488.

Cyclic AMP ELISA

Total cell lysates, prepared in 0.1M HCl, and standards and cAMP AChE Tracer were added to pre-coated plates in duplicate using the cyclic AMP ELISA kit from Cayman (Cat#581001, RRID:AB_3095671) and incubated for 18 hours at 4°C. Plates were washed five times and treated with Ellman's Reagent for a period of 90-120 minutes, followed by optical density quantification at 405nm and 420nm against the standard curve.

Flow cytometry

Single cell suspensions were washed twice by FACS buffer (2% FBS, DPBS). FACS were performed on BD Accuri C6 Plus and analyzed by FlowJo_V10 (RRID:SCR_008520). Live cells were separated from debris using an SSC-A (y) vs. FSC-A (x) dot plot. FSC-A (x) lattice plots, FSC-H (y) and FSC-A (x)/SSC-H (y) vs. SSCA (x) lattice plots were used to exclude doublets. Singlets were gated and analyzed as shown in the diagram in the article.

Intracranial GSC implantation

All animal experiments were performed in adherence to the regulations and guidelines set by the institutional IACUC. For the L2, CA3, and CA7 lines, an initial serial dilution injection was conducted to assess the tumorigenic potential of each line. Cells in serial quantities of 10^3, 10^4, and 10^5 were implanted into 5 NSG mice and the lowest cell number needed to induce brain tumor formation within 50 days post-injection was determined as followed: 10^4 cells for L2 and CA3, and 10^5 for CA7. Due to the limited availability of GSC23, GSC122, and GSC33 cells, 10^4 cells were injected into each mouse. All lines were suspended in 3µl of PBS for implantation into the posterior frontal lobe of 6-week-old NSG mice (Jackson Laboratory, RRID:IMSR_JAX:005557). Equal numbers of both male and female mice were used in each experiment. Injection was performed with an automated mouse stereotaxic apparatus (Stoelting's, RRID:SCR_025303) at the rate of 1µl/min and 2 mm lateral to the right and 3.5 mm deep, using bregma as a reference. Post-injection, mice were meticulously monitored for postop complications and followed for survival.

Tumor samples

We obtained and performed bulk RNA-seq of 7 pairs of primary and recurrent GBM tumors from 6 patients who were treated with standard chemoradiation followed by adjuvant TMZ and TTFields treatment and subsequently experienced tumor recurrence that was pathologically confirmed following either resection or biopsy. One patient had 2 separate recurrences located in 2 different locations (right and left occipital lobes). For comparison, we sourced an external dataset from the European Genome-phenome Archive (EGAC00001002176, RRID:SCR_004944) and accessed with the generous permission from Ilan Volovitz (30). This dataset is comprised of paired primary and current tumor tissues from 6 newly diagnosed GBM

13

patients, treated with standard chemoradiation followed by adjuvant TMZ alone. We processed the FASTQ data using the same pipeline as our bulk RNA-seq analyses. The resultant TPM data was then employed for a comparative gene expression analysis for EP3 and ZNF488.

Statistical Analyses

Statistical analysis was performed using GraphPad Prism 10 software (RRID:SCR_002798). All Student's t-tests were two-sided, and P values ≤0.05 (with 95% confidence intervals) were considered statistically significant for each specific statistical comparison (*$P < 0.05$. **$P < 0.01$, ***$P < 0.001$). In cases of multiple comparisons, adjustments were made using one-way ANOVA. Continuous outcome data are presented as mean ± S.E.M. For mouse survival data, the Log-rank (Mantel-Cox) test was employed, with adjustments made based on groups. For all box and whisker plots, the whiskers are the minimum and maximum values, the lower and upper box edges the 25th and 75th percentage values, respectively, and the lines within the boxes the median.

Study approval: All animal experiments were approved by the IACUC at the University of Southern California and the University of Florida and performed in compliance with all ethical regulations regarding animal research. For GSC and GBM tumor tissues, the study was approved by the IRB of the University of Florida and conducted in accordance with the Declaration of Helsinki ethical standards. Written informed consent was obtained from three patient at the initial diagnosis and at first recurrence following standard treatment for collection and immediate processing of fresh brain tumor samples at the time of surgical resection.

Data Availability: The RNA-seq data generated in this study is available in the Gene Expression Omnibus (GEO) at accession number GSE270513. The results published here are in whole or part based upon data generated by the TCGA Research Network: https://www.cancer.gov/tcga. The GeneRep–nSCORE algorithm code can be accessed in GitHub at: https://github.com/TranLabUSC/NETZEN-classic. All other raw data are available from the corresponding author upon request.

Results

Generation and characterization of TTFields-resistant GBM cells.

To generate TTFields-resistant GBM cells, we utilized the Inovitro™ system to treat GBM cells continuously with TTFields (200 kHz unless otherwise noted) until resistance emerged. To ensure that changes in proliferation were not due to culture confluency and to assess gene expression changes as resistance developed, cells were reseeded at the same density every seven days (7D) of TTFields treatment to maintain a constant growth condition with a two-day break to allow them to recover before each new cycle. We counted live cells on days two, four, and seven of each cycle and collected total RNA for RNA-sequencing (RNA-seq) from the remaining cells after reseeding (**Figure 1A**). Each cell line underwent up to five treatment cycles. Control cells were subjected to the same number of cycles without TTFields treatment (non-TTFields-treated or NT). We focused initially on three established GBM cell lines LN428,

LN827 and U87 to identify resistance mechanism with plans to validate findings in patient-derived GSC. GSC, maintained in serum-free stem cell culture conditions, exhibited poor tolerance of frequent passaging under continuous TTFields, complicating treatment continuity. We selected the three established GBM lines for their TTFields sensitivity at baseline and to represent two major GBM subtypes — mesenchymal (LN827, U87) and proneural (LN428) (31-33). During the first 14D of treatment, cell growth was markedly suppressed by TTFields compared to non-treated controls in all three GBM lines. By 21D, however, the cells gradually regained proliferative capacity despite under continuous TTFields exposure. Between 28–35D, their proliferation rates approached or overlapped with those of non-treated cells (**Figure 1B**). For all subsequent experiments, TTFields-resistant (R) cells were defined as those treated with TTFields continuously for at least 28–35D and maintained under continuous TTFields unless otherwise specified, with the non-treated parental cells serving as their sensitive counterparts.

TTFields treatment failure may occur due to resistance to its physical forces, such as changes in cell size to alter the cell's dielectric properties (11-13), or to the subsequent biological effects of the physical insults, or both. To explore these possibilities, we compared size distributions of TTFields-resistant cells and their non-treated sensitive counterparts via cytometric forward scatter, finding no significant differences (Supplemental Figure 1A). This suggests that changes in cell size are unlikely a major resistance mechanism in the three GBM lines. We then evaluated the frequency of cytosolic naked micronuclei clusters, caused by TTFields-induced nuclear envelope disruption (10), in both resistant and non-treated sensitive cells. Although two resistant lines (LN428 and U87) showed lower frequencies compared to non-treated cells, resistant cells still exhibited high frequencies of cytosolic micronuclei clusters compared to non-treated cells, indicating continued susceptibility to nuclear envelope injury

16

(Supplemental Figure 1B). Additionally, shRNA depletion of cytosolic DNA sensors STING and AIM2, downstream of cytosolic micronuclei clusters, did not affect resistant cells' susceptibility to TTFields' cytotoxicity (Supplemental Figure 1C). These findings suggest that TTFields resistance likely involves pathways downstream or distinct from the initial physical injuries rather than being a direct response to them.

EP3 is a master regulator of cellular resistance to TTFields.

To identify pathways associated with TTFields resistance, we conducted a comprehensive temporal RNA-seq analysis (sequencing summaries in Supplemental Table S1) of the three GBM lines under continuous TTFields treatment at 0D (NT), 7D (early changes), and 28–35D (late changes). Significant gene expression changes were observed in all three resistant GBM lines at 28–35D, compared to the NT control. Interestingly, similar patterns of gene expression changes were detected as early as 7D, even when cells were still sensitive to TTFields (**Figure 1C**), indicating that the resistance mechanisms are already in motion well before resistance becomes experimentally evident. We then employed GeneRep–nSCORE, a robust gene network-based machine learning algorithm that identifies master regulators responsible for network perturbations (34). This analysis, enhanced by fully automated and annotated visualization based on Gene Ontology pathways (35), identified several large regulatory hubs associated with self-renewal (stemness), migration, and immune effects, which were significantly upregulated in TTFields-resistant cells compared to their sensitive counterparts (**Figure 1D-E** and Supplemental Figure S1D). Temporal analysis revealed that the migration-related hub 1.9 and the larger of the two immune-related hubs (hub 1.6) began to rise in response to TTFields only after 7D. Hub 1.6 encompasses key regulators involved in innate

and adaptive immune responses, including those related to T1IFN signaling and viral antigen-associated immunity (Supplemental Figure S2). This delayed activation of hub 1.6, compared to the faster-responding inflammation-related hub 1.8, aligns with the persistent formation of cytosolic micronuclei clusters post-TTFields treatment, which are known to stimulate adaptive immunity in GBM (10). In contrast, hub 1.8, which was upregulated more rapidly by 7D, is enriched in genes involved in pathologic immune responses (**Figure 1D-E**, Supplemental Figure S1D), recruitment of inhibitory immune cells, and mechanisms of immune escape (Supplemental Figure S3). Thus, a critical aspect of the resistance program is the activation of regulatory networks that counter both anti-mitotic effects of TTFields and its potential to trigger immune responses.

The self-renewal (stemness) hub 1.5, which contains neural development pathways, is the largest and most rapidly upregulated hub (by 7D) in response to TTFields. The enrichment of master regulators controlling stemness of GBM cells likely plays a crucial role in resistance development. Notably, PTGER3 or EP3, a key regulator within this hub, consistently ranks among the top master regulators across all three TTFields-resistant GBM lines, showing increased network dominance after just 7D of treatment in two lines (Supplemental Table S2 and the complete nSCORE ranking evolution of all master regulators in Supplemental Table S3), indicating early initiation of the resistance program. In fact, EP3 mRNA expression was swiftly upregulated within 6 hrs of TTFields exposure in all three GBM lines and continued to rise as resistance developed (**Figure 1F**), a trend confirmed at the protein level in resistant cells (**Figure 1G**).

To validate EP3 upregulation in patient-derived GSC during the development of TTFields resistance, we generated TTFields-resistant GSC from the L2, CA3, and CA7 GSC

lines (10) by subjecting them to continuous TTFields treatment for at least 35 days until resistance emerged. This process was performed without regular replating intervals, due to the prolonged recovery time required under stem cell culture conditions with continuous TTFields exposure. GSC viability was assessed by the number and size of spheres formed in stem cell media, reflecting metrics of GSC's self-renewal and progenitor cells' proliferative capacity (36), respectively (**Figure 1H**). To further confirm EP3's role in TTFields resistance, we analyzed regulatory networks derived from the RNA-seq profiles of the three TTFields-resistant GSC lines and their non-treated sensitive counterparts using the GeneRep–nSCORE algorithm (34). In resistant GSC, EP3 was upregulated and occupied a central position in the network, linked directly and indirectly (via ZNF488) to key functional hallmarks — Self-renewal, Metabolism and Cell Growth, and Migration and Invasion (37) — of the GSC regulatory network (**Figure 1I**). These findings suggest that EP3 may be a master regulator of TTFields resistance in GSC. EP3 upregulation in TTFields-resistant GSC was verified by qPCR and immunoblotting (**Figure 1J-K**), with no significant changes in cell size between resistant and sensitive states (Supplemental Figure S4A). However, TTFields-resistant GSC exhibited lower rates of cytosolic micronuclei cluster formation after 24-hr TTFields exposure compared to their non-treated sensitive counterparts, indicating higher resistance to TTFields' physical forces (Supplemental Figure S4B).

In the phospholipids/arachidonic acid pathway, EP3 has the highest affinity (i.e., lowest dissociation constant K_d) for PGE2 among the four PGE2 receptors (**Figure 2A**). EP3 can be blocked indirectly by inhibiting the upstream enzyme cyclooxygenase 1/2 (COX1/2) using aspirin or directly with highly potent, specific EP3 inhibitors (EP3i) like L798,106 and DG041. EP3 is also the only PGE2 receptor coupled with the inhibitory Gα protein, which reduces

cAMP production by deactivating adenylyl cyclase (38). TTFields-resistant GBM cells with higher EP3 expression showed lower cAMP levels compared to non-treated cells, with a significant difference observed in U87 cells. Moreover, cAMP levels in resistant cells consistently rebounded when treated with EP3i L798,106 (500nM) or DG041 (50nM) (Supplemental Figure S5). All the selected drug concentrations in this and subsequent studies were based on those above their respective IC_{50}'s that did not negatively affect cell growth in the three GBM lines after 72-hrs treatment (Supplemental Figure S6).

To validate EP3's role as a master regulator in TTFields resistance, we employed three approaches across the six GSC and established GBM lines. First, we inhibited EP3 in TTFields-resistant cells using 0.5mM aspirin, 50nM DG041, or 500nM L798,106 (**Figure 2B-D** and Supplemental Figure S7A-C) or through depletion with two independent *EP3* shRNA (*shEP3-1* and *shEP3-2*) starting 24 hrs prior to and during the 3-day exposure to TTFields (**Figure 2E** and Supplemental Figure S7D). All approaches restored sensitivity to TTFields across the six TTFields-resistant lines, compared to the vehicle-treated or *shScrambled* controls (**Figure 2B-E** and Supplemental Figure S7A-D), with aspirin, an indirect EP3 pathway inhibitor, showing slightly lower reversal rates compared to the other agents.

Second, we overexpressed EP3 in TTFields-sensitive cells using a lentiviral vector and measured their resistance to TTFields compared to empty virus (ev) controls. While EP3 overexpression alone did not affect sphere number, size, or cell growth, it induced relative resistance to 3-day TTFields treatment in both GSC (**Figure 2F**) and established GBM (Supplemental Figure S7E) lines, measured as fractions of remaining spheres and cells, respectively, in the TTFields-treated over NT controls. The acquired resistance was more pronounced in the GBM lines than in GSC, which already expressed high EP3 levels at baseline.

Third and most importantly, we co-treated all six GBM (**Figure 3A**) and GSC (**Figure 3B**) lines with TTFields and the EP3i L798,106 to determine if resistance could be prevented over 35 days. Concomitant EP3i treatment preemptively averted resistance altogether, maintaining sensitivity to TTFields throughout the 35-day treatment in all six GBM and GSC lines compared to vehicle-treated controls. Notably, prolonged treatment with L798,106 alone did not affect cell growth or sphere formation, suggesting minimal off target effects.

In summary, EP3 is a key master regulator of the TTFields resistance program in GBM cells and GSC, and represents a potential therapeutic target to enhance, sustain, and restore sensitivity to TTFields' cytotoxic effects.

EP3 promotes self-renewal and tumorigenicity of GSC in TTFields resistance development.

Given that EP3 is the top-ranked master regulator within the rapidly upregulated self-renewal hub in resistant GBM cells (**Figure 1D-E**), plays a pivotal role in the regulatory network of resistant GSC, and its inhibition reduces sphere formation in TTFields-resistant GSC (**Figure 2E**), we further investigated its role in regulating self-renewal and *in vivo* tumorigenicity — critical markers of tumor-initiating potential — in GSC (39). To address these questions, we first examined whether EP3 is necessary for non-GSC GBM cells, which typically grow as adherent cells in serum-rich media, to shift toward spherical growth in serum-free stem cell media. Stem cell cultures from TTFields-resistant LN827-R and U87-R lines exhibited a substantial increase in both sphere count and size compared to their non-treated sensitive counterparts (Supplemental Figure S8A). Upon treatment with the EP3i L798,106 under 72-hr continuous TTFields exposure, both sphere number and size in LN428-R and U87-R cells were markedly reduced

21

(Supplemental Figure S8B). These findings suggest that TTFields resistance is associated with enhanced self-renewal capabilities, which requires functional EP3.

In GSC cultured as spheres in serum-free stem cell media, we compared the expression of two key GSC markers, aldehyde dehydrogenase 1 family member A1 (ALDH1A1) (40) and CD133 (41), via cytometry in TTFields-resistant and non-treated sensitive GSC, with or without EP3 depletion. TTFields-resistant GSC showed significantly higher levels of these markers compared to non-treated cells (**Figure 4A-B**). EP3 depletion using either of the two *shEP3* shRNA consistently reduced the expression of these markers in both sensitive and resistant GSC, with a more pronounced reduction, especially in ALDH1A1, observed in resistant GSC (**Figure 4A-B**). Next, we compared the effects of the EP3i L798,106 combined with TTFields treatment on sphere-forming frequency and *in vivo* tumorigenicity of TTFields-resistant GSC to their non-treated sensitive counterparts. The orthotopic brain implantation entailed injecting equal numbers of GSC into the posterior right frontal lobes of 6-week-old immunocompromised NOD/SCID/gamma (NSG) mice with equal numbers of males and females. L798,106 or the vehicle was also added to the cells before implantation, following a 72-hr treatment in culture. We confirmed neurological signs and the presence of tumors at the original injection site in each animal at the time of death or a predefined humane endpoint to accurately record disease-free survival. In TTFields-sensitive GSC, L798,106 treatment, with (Vehicle+TTF3D vs L798+TTF3D) or without (Vehicle+NT vs L798+NT) 3-day TTFields exposure, had minimal effects on both sphere-forming frequency and orthotopic tumorigenicity compared to vehicle treated controls (**Figure 4C-H**), except for CA7 GSC, where EP3i resulted in a slight reduction in sphere-forming frequency but a significant increase in survival. This effect is likely due to the higher basal EP3 expression and thus relatively higher TTFields resistance in CA7 (**Figure 1K**).

In contrast, animals that received L798,106-treated TTFields-resistant cells showed a moderate reduction in self-renewal (**Figure 4C-E**), but significantly higher rates of overall survival compared to vehicle-treated controls (**Figure 4F-H**). This confirms the efficacy of targeting EP3 to reverse TTFields resistance and reduce *in vivo* tumorigenicity in GSC.

To confirm EP3's role in the tumorigenic potential of GSC, we generated three additional patient-derived GSC lines freshly isolated from TTFields-resistant GBM tumors with minimal *in vitro* culturing to avoid confounding effects from extensive passaging. We performed sphere formation, orthotopic tumorigenicity, and survival analysis with or without L798,106 treatment, similar to previous experiments (**Figure 5A**). These resistant tumors were resected after 4 (GSC122), 16 (GSC33), and 21 (GSC23) months of continuous adjuvant TTFields, which also included up to 12 months of maintenance temozolomide (TMZ). To account for potential delayed tumor latency of freshly isolated GSC in NSG mice, survival monitoring was extended, but only to a maximum of 250 days post-implantation, avoiding confounding effects from spontaneous deaths typically occurring in NSG mice around 9 months of age. All three freshly isolated GSC expressed higher to similar EP3 mRNA levels compared to the resistant L2-R, CA3-R, and CA7-R cells (**Figure 5B**). L798,106 treatment significantly or nearly significantly reduced sphere number and/or size after 3-day TTFields exposure, as measured by single-cell sphere formation (**Figure 5C-E**) and extreme limiting dilution (Supplemental Figure S9) assays, as well as *in vivo* tumorigenicity (**Figure 5F-H**). Notably, while L798,106 treatment alone did not affect sphere-forming capacity, it significantly reduced *in vivo* tumorigenicity and improved survival in GSC122 to the same degree as those implanted with low-sphere-forming L798,106+TTF3D cells (**Figure 5F**). For GSC23, at the 250-day post-implantation termination point, all five animals receiving either L798,106 or L798,106+TTF3D cells were still alive,

whereas two of five vehicle-treated and one of five Vehicle+TTF3D-treated animals had succumbed by 200 days (**Figure 5H**). While these results in GSC23 did not reach statistical significance due to early termination, they were consistent with findings in the other two freshly isolated resistant GSC models.

In summary, EP3 regulates TTFields resistance by promoting self-renewal and *in vivo* tumorigenicity potentials of GSC in GBM.

The neural stem cell factor ZNF488 mediates TTFields resistance in GBM cells.

Thus far, our findings suggest that the GPCR EP3 functions as a master regulator of the TTFields resistance program by enhancing GSC self-renewal and tumorigenicity. Typically, master regulators are nuclear transcription factors that directly control transcription of numerous target genes. In the regulatory network of resistant GSC, EP3 is directly linked to the neural stem cell nuclear factor ZNF488 (42), which has extensive connections to the self-renewal (stemness) hub (**Figure 1I**). This indicates that ZNF488 could be the key link in this mechanistic pathway. To validate the potential cooperation between EP3 and ZNF488, we examined the temporal evolution of the EP3-regulated resistance subnetwork during continuous TTFields treatment in the three established GBM lines using the GeneRep–nSCORE algorithm (34). Compared to non-treated controls, EP3 was upregulated early, with the nascent EP3-dependent self-renewal or stemness hub emerging by 1D of treatment, increasing by 7D, and reinforcing further by 28–35D (**Figure 6A-D**). In contrast, ZNF488 was initially downregulated after 1D (**Figure 6A,** purple arrow) but showed increased expression and importance in the self-renewal hub by 7D (**Figure 6B,** purple arrow), indicating its secondary role to EP3 in initiating resistance. By 28–35D,

24

ZNF488, along with EP3, was sharply upregulated and established as a top-ranked regulator in the self-renewal hub (**Figure 6C-D,** broken circles), becoming top ten of all genes and hubs and the top two upregulated factors of the consolidated self-renewal hub (Supplemental Table S4). This finding identifies ZNF488 as the mechanistic link between membrane-bound EP3 and the nuclear transcriptional program driving TTFields resistance. In the three GSC lines L2, CA3, and CA7, ZNF488 was significantly upregulated at both mRNA (**Figure 6E**) and protein (**Figure 6F**) levels in resistant cells compared to their non-treated sensitive counterparts. Depletion of ZNF488 mRNA using two independent shRNA (*shZNF488-1* and *shZNF488-2*), confirmed by immunoblotting, effectively re-sensitized all three TTFields-resistant GSC lines (**Figure 6G** and Supplemental Figure S10A) and three established resistant GBM lines (Supplemental Figure S10B-C) to 3-day TTFields treatment, compared to the control scrambled shRNA (*shScr*). In non-treated sensitive GSC, ZNF488 depletion alone reduced sphere-forming frequency but not proliferative capacity (sphere size), likely due to its role in neural stem cells, and increased TTFields-dependent suppression in L2 and not CA3 and CA7 GSC.

To further dissect ZNF488's evolving role in resistance, we extracted the subnetwork with direct links to ZNF488 from all cell lines (**Figure 6H**). As predicted, ZNF488 directly regulates the three hallmark hubs of GSC — Self-renewal (stemness), Metabolism and cell growth, and Migration and invasion (37). Depletion of ZNF488 in the three GSC lines using *shZNF488-1* impacted eight key factors controlling these hubs, with the two most dominant factors SLC2A4RG (metabolism and cell growth) and ETV4 (self-renewal), showing consistent changes in all three lines (**Figure 6I**).

Overall, these results strongly validate the critical regulatory role of ZNF488 in the EP3-dependent TTFields resistance program.

EP3 is localized to the nuclear envelope in response to TTFields and interacts with ZNF488 to induce TTFields resistance.

Next, we aimed to resolve the second mechanistic conundrum of how EP3, a GPCR, and ZNF488, a nuclear factor, interact or if they independently regulate resistance. Confocal microscopy of the three established GBM lines exposed to 24-hr TTFields revealed a significant increase in EP3's nuclear presence, particularly co-localizing with the nuclear envelope marked by lamins A and C (LaminAC) (43) (**Figure 7A** and Supplemental Figure S11A). This suggests a plausible interaction site for the two master regulators. EP3 was present in both cytosolic and nuclear compartments in resistant cells, while ZNF488 was primarily nuclear, setting up a potential physical interaction, which was confirmed by immunofluorescence (**Figure 7B** and Supplemental Figure S11B) and subcellular fractionation (**Figure 7C**). Color pixel intensity co-registration further confirmed EP3–ZNF488 co-localization mainly in the nucleus of resistant cells (Supplemental Figure S12). In TTFields-induced cytosolic micronuclei clusters, EP3 and ZNF488 showed limited overlap, likely due to the absence of a nuclear envelope (10).

Mechanistically, EP3 and ZNF488 form a nuclear complex, demonstrated by their specific co-immunoprecipitation from nuclear fractions of TTFields-resistant GBM cells and GSC (**Figure 7D**). To dissect this interaction, we engineered EP3 and ZNF488 mutants tagged with the 6xHis and Flag epitopes, respectively, and mapped their interacting domains via co-immunoprecipitation in 293 cells. EP3's N-terminus is located within the nuclear envelope's intermembrane space, topographically equivalent to the extracellular space, while its C-terminus and internal loops 1-3 (IL1-3) extend into the nucleoplasm, with IL2 serving as the Gαi binding site (44) (**Figure 7E**). EP3's C-terminus has been shown to interact with various second

messengers depending on cellular contexts (45, 46). Consistent with our hypothesis that EP3 binds ZNF488 in the nucleoplasm, deletion of either the IL2 (EP3-IL2) or C-terminal (EP3-C) domain of EP3 severely reduced its interaction with full-length ZNF488 (FL-ZNF488), while an EP3 mutant lacking the N-terminus (EP3-N) still co-immunoprecipitated with FL-ZNF488 (**Figure 7F**, top). ZNF488 contains a repression domain (RD) in the middle and a zinc finger domain (ZF) at the C-terminus for binding to target gene promoters (47). We found that the ZF domain is essential for ZNF488 to bind full-length EP3 (FL-EP3), as a ZNF488 mutant lacking the ZF domain (ZNF488-ZF) failed to interact with EP3, whereas one lacking the RD domain (ZNF488-RD) retained this ability (**Figure 7F**, bottom). To confirm that the EP3–ZNF488 complex is both necessary and sufficient for TTFields resistance, we expressed various combinations of full-length proteins and truncated mutants (EP3-C and ZNF488-ZF) in TTFields-sensitive L2 GSC and evaluated their response to 24-hr TTFields treatment. In non-TTFields-treated L2 cells (NT), none of the combinations affected self-renewal, but only the co-expression of FL-EP3 and FL-ZNF488 conferred resistance to TTFields. In contrast, neither EP3-C nor ZNF488-ZF were sufficient to induce resistance (**Figure 7G**), underscoring the importance of the full-length EP3–ZNF488 complex in mediating resistance. Lastly, we tested whether EP3i, like L798,106, could disrupt the EP3–ZNF488 interaction as a potential mechanism of action. Treatment with L798,106 resulted in a dose-dependent reduction of the EP3–ZNF488 complex (**Figure 7H**).

Taken together, EP3 localizes to the nuclear envelope in response to TTFields treatment, where it forms a complex with ZNF488 to establish TTFields resistance in GBM. The EP3–ZNF488 interaction is necessary and sufficient in inducing the resistance program.

Epistasis of the EP3–ZNF488 regulatory axis

Given the transcriptional role of the EP3–ZNF488 complex, we examined their epistatic interactions in regulating TTFields resistance in GBM. In all six GSC and established GBM lines, shRNA-mediated depletion of ZNF488 in EP3-overexpressing cells effectively reversed EP3-induced resistance, while EP3 depletion overcame ZNF488-induced resistance to 3-day of TTFields treatment (**Figure 8A** and Supplemental Figure S13A-B). Notably, these interactions were consistent across the three established GBM lines, regardless of culture conditions — whether in serum-repleted adherent cells or serum-free spheres (Supplemental Figure S13). In non-TTFields-treated controls, growth rate differences were inconsistent under these conditions.

To confirm the upregulation of the EP3–ZNF488 axis in TTFields-resistant GBM tumors, we analyzed bulk RNA-seq from six newly diagnosed GBM patients treated with standard chemoradiation followed by adjuvant TMZ plus continuous TTFields. All patients developed histologically confirmed recurrences, with one patient having two separate recurrent tumors. For comparison, we sourced an independent dataset of six paired primary-recurrent samples from GBM patients treated with standard chemoradiation and adjuvant TMZ alone (30) (Supplemental Table S5). In recurrent tumors treated with TMZ plus TTFields, both EP3 and ZNF488 were significantly upregulated compared to pre-treatment primary tumors, while recurrent tumors treated with TMZ alone showed a slight, non-significant reduction in both markers (**Figure 8B-C**). This upregulation is likely not due to TMZ, as TMZ treatment alone did not alter EP3 expression in the three GSC lines, and its impact on ZNF488 was cell line-dependent (Supplemental Figure S14A-B). Additional, TTFields resistance did not affect susceptibility to the cytotoxic effects of TMZ (Supplemental Figure S14C).

The epistatic cooperation between EP3 and ZNF488 in GSC prompted us to explore whether this regulatory axis represents a broader response to TTFields and a novel pathway for therapeutic resistance in other cancers. Notably, across eight lines of various human and murine cancers, we observed statistically significant upregulation of EP3 mRNA in all lines and ZNF488 mRNA in six, following 24-hr TTFields exposure (**Figure 8D**). Moreover, in at least five cancer types where TTFields is not a standard treatment, high co-expression of EP3 and ZNF488 in primary tumors correlated with reduced survival compared to tumors with low expression of both genes (**Figure 8E**). This suggests that the EP3–ZNF488 axis negatively impacts prognosis in multiple cancers. In cancers like GBM, which exhibits low baseline expression, continuous TTFields exposure may activate this axis, promoting therapy resistance.

In conclusion, this study uncovers a coherent mechanism of TTFields resistance in GBM, where EP3 upregulation shortly after TTFields exposure leads to its nuclear envelope localization and physical and epistatic cooperation with ZNF488. This interaction enhances GSC self-renewal and tumorigenicity, increasing resistance to TTFields. Moreover, the EP3–ZNF488 axis may serve as a prognostic marker for therapeutic resistance across various cancers.

Discussion

Therapeutic resistance is a major challenge in cancer treatment, leading to tumor progression and early mortality. TTFields have shown promise in overcoming various therapeutic barriers, but prolonged application eventually results in resistance. Identifying a single mechanism behind TTFields resistance has been difficult due to their multifaceted

antitumor actions. While changes in cell size and dielectric properties were proposed as potential mechanisms, our study found no significant size differences between TTFields-resistant and non-treated sensitive cells. Instead, we identified a more complex molecular program driven by EP3–ZNF488 cooperation. We used established GBM cell lines to generate resistant cells and identify the resistance pathway due to their ease in repeated passages under TTFields treatment. To address the physiological limitations of these cells, we validated key findings in patient-derived GSC, including those freshly isolated from TTFields-resistant tumors, both *in vitro* and *in vivo*. The pivotal Phase 3 clinical study showed TTFields plus TMZ chemotherapy resulted in a median PFS of 6.7 months (1), much longer than the 4-5 weeks for TTFields resistance to emerge *in vitro*. Determining the exact timing of resistance emergence *in vivo* is challenging due to tumor-specific factors like doubling time and radiographic appearance, and whether resistance was to TTFields, TMZ, or both. Supporting our TTFields resistance model, we observed significant increases in EP3 and ZNF488 in recurrent tumors compared to pre-treatment primary tumors in a small cohort of patients treated with TTFields plus TMZ, while no such increases were observed in an independent cohort treated with TMZ alone. Our results also show that TTFields-resistant GSC remain susceptible to TMZ cytotoxicity, suggesting distinct resistance mechanisms for these 2 modalities. However, to definitively confirm that the EP3–ZNF488 axis in GSC is essential for TTFields resistance and to differentiate TTFields resistance from TMZ resistance, an orthotopic continuous TTFields treatment system in GSC xenografts, with or without TMZ alone, followed by validation using tumor samples from a larger patient cohort, will be required.

The localization of EP3, a seven-transmembrane GPCR involved in various physiological responses, to the nuclear envelope aligns with its dynamic role in cellular processes and supports

30

previous findings in normal endothelial cells (48, 49). It remains unclear whether EP3's nuclear envelope localization in TTFields-resistant cells results from plasma membrane translocation via internalized vesicles or direct delivery of newly synthesized EP3 from the ER. ER stress induced by TTFields (8) or other treatments may enhance EP3 delivery to the nuclear envelope. Different EP3 isoforms, with distinct C-terminal regions, have been suggested to target various subcellular locations, including the nuclear envelope (50), aligning with our finding that EP3's C-terminus is required for ZNF488 interaction. Molecular tracking and high-resolution imaging in TTFields-exposed cells will be needed to explore these possibilities further. Our results also indicate that the EP3–ZNF488 axis directly enhances GSC self-renewal and *in vivo* tumorigenicity. This GSC-centered resistance mirrors general resistance mechanisms in various cancers, where cancer stem-like cells (CSC) are central to resistance against both pharmaceutical and physical treatments (51, 52), with the EP3/ZNF488 axis as a novel addition. ZNF488, as a transcriptional repressor, likely exerts its effects by binding to target gene promoters via its zinc finger domain (47). EP3 may interact with ZNF488's zinc finger domain, disrupting its binding to CSC-associated gene regulatory elements, thereby initiating resistance. To validate this hypothesis, cataloging target gene de-repression by the EP3–ZNF488 complex compared to ZNF488 alone using techniques like chromatin IP sequencing, followed by experimental validation, will be essential.

We observed the same EP3–ZNF488 co-expression in multiple cancer cell lines of different origins in response to TTFields and uncovered its correlation with reduced survival in several cancer types. This suggests the EP3–ZNF488 cooperation may be a common prognostic marker and a key regulatory axis of CSC. Resistance may arise from selecting pre-existing resistant CSC subclones or remodeling the regulatory network in sensitive cells. The early

upregulation of EP3 shortly after TTFields exposure in GBM cells — well before resistance emerges — supports the network reconstruction model. Temporal analysis of early regulatory gene expression changes following TTFields treatment is needed to determine how quickly EP3's network importance rises, however. Additionally, the upregulation of two immune regulatory hubs with potentially opposing effects — one promoting adaptive anti-tumor immunity and the other fostering inflammation — raises important questions about their interaction and influence on the overall immune response induced by TTFields. Understanding these interactions is crucial for enhancing the anti-tumor immune response while mitigating maladaptive inflammation induced by TTFields. In syngeneic GBM models, short TTFields treatment (3 days) induced adaptive immune activation (10). For immunotherapeutic purposes, short TTFields pulses may achieve these goals without the resistance risk from prolonged application, but this concept needs testing in animal models and patients.

Finally, the therapeutic implications of our findings are significant. Inhibiting the EP3–ZNF488 axis to prevent TTFields resistance suggests a strategy for combinatory therapies to extend the efficacy of TTFields and other cytotoxic treatments. Although EP3i have not been tested in cancer patients, the selective EP3i DG401 has demonstrated safety in mice and healthy humans by reducing platelet aggregation without affecting hemostasis (53, 54), suggesting potential safety for this approach in cancer patients. Alternatively, COX1/2 inhibitors like aspirin can partially re-sensitize TTFields-resistant GSC and targeting the EP3–ZNF488 interaction in GSC may be effective. This study opens avenues for future research into agents that can efficiently and safely target this new CSC axis in GBM and other cancers.

Author contributions

D.C., S. B. L. and D.D.T. conceived and performed experiments and wrote the manuscript. D.D.T. secured funding. T.E.H., H.M., T.L., and A.O performed experiments or provided technical support. B.S. provided technical genomics expertise and contributed to manuscript writing.

Acknowledgements

References

1. Stupp R, Taillibert S, Kanner A, Read W, Steinberg D, Lhermitte B, et al. Effect of tumor-treating fields plus maintenance temozolomide vs maintenance temozolomide alone on survival in patients with glioblastoma: a randomized clinical trial. *JAMA.* 2017;318(23):2306-16.

2. Ceresoli GL, Aerts JG, Dziadziuszko R, Ramlau R, Cedres S, van Meerbeeck JP, et al. Tumour Treating Fields in combination with pemetrexed and cisplatin or carboplatin as first-line treatment for unresectable malignant pleural mesothelioma (STELLAR): a multicentre, single-arm phase 2 trial. *The Lancet Oncology.* 2019;20(12):1702-9.

3. Leal T, Kotecha R, Ramlau R, Zhang L, Milanowski J, Cobo M, et al. Tumor Treating Fields therapy with standard systemic therapy versus standard systemic therapy alone in metastatic non-small-cell lung cancer following progression on or after platinum-based therapy (LUNAR): a randomised, open-label, pivotal phase 3 study. *The Lancet Oncology.* 2023;24(9):1002-17.

4. Kirson ED, Dbaly V, Tovarys F, Vymazal J, Soustiel JF, Itzhaki A, et al. Alternating electric fields arrest cell proliferation in animal tumor models and human brain tumors. *Proc Natl Acad Sci U S A.* 2007;104(24):10152-7.

5. Kirson ED, Gurvich Z, Schneiderman R, Dekel E, Itzhaki A, Wasserman Y, et al. Disruption of cancer cell replication by alternating electric fields. *Cancer Res.* 2004;64(9):3288-95.

6.   Giladi M, Munster M, Schneiderman RS, Voloshin T, Porat Y, Blat R, et al. Tumor treating fields (TTFields) delay DNA damage repair following radiation treatment of glioma cells. *Radiat Oncol.* 2017;12(1):206.

7.   Karanam NK, Ding L, Aroumougame A, and Story MD. Tumor treating fields cause replication stress and interfere with DNA replication fork maintenance: Implications for cancer therapy. *Transl Res.* 2020;217:33-46.

8.   Shteingauz A, Porat Y, Voloshin T, Schneiderman RS, Munster M, Zeevi E, et al. AMPK-dependent autophagy upregulation serves as a survival mechanism in response to Tumor Treating Fields (TTFields). *Cell Death Dis.* 2018;9(11):1074.

9.   Chang E, Patel CB, Pohling C, Young C, Song J, Flores TA, et al. Tumor treating fields increases membrane permeability in glioblastoma cells. *Cell Death Discovery.* 2018;4(1):113.

10.   Chen D, Le SB, Hutchinson TE, Calinescu A-A, Sebastian M, Jin D, et al. Tumor Treating Fields dually activate STING and AIM2 inflammasomes to induce adjuvant immunity in glioblastoma. *J Clin Invest.* 2022;132(8).

11.   Kirson ED, Dbalý V, Tovaryš F, Vymazal J, Soustiel JF, Itzhaki A, et al. Alternating electric fields arrest cell proliferation in animal tumor models and human brain tumors. *Proceedings of the National Academy of Sciences.* 2007;104(24):10152-7.

12.   Wenger C, Miranda PC, Salvador R, Thielscher A, Bomzon Z, Giladi M, et al. A Review on Tumor-Treating Fields (TTFields): Clinical Implications Inferred From Computational Modeling. *IEEE Reviews in Biomedical Engineering.* 2018;11:195-207.

13.   Miranda CWaPC. In: Wong ET ed. *Alternating Electric Fields Therapy in Oncology A Practical Guide to Clinical Applications*

of Tumor Treating Fields Switzerland: Springer; 2016.

14.   Schneiderman RS, Giladi M, Porat Y, Munster M, Weinberg U, Kirson ED, et al. Overcoming cell size escape from tumor treating fields using a varying frequency treatment paradigm in vitro. *Journal of Clinical Oncology.* 2013;31(15_suppl):e22134-e.

15.   Di Gregorio E, Israel S, Staelens M, Tankel G, Shankar K, and Tuszyński JA. The distinguishing electrical properties of cancer cells. *Phys Life Rev.* 2022;43:139-88.

16.   Ruan YC, Zhou W, and Chan HC. Regulation of Smooth Muscle Contraction by the Epithelium: Role of Prostaglandins. *Physiology.* 2011;26(3):156-70.

17.   Mawhin MA, Tilly P, and Fabre JE. The receptor EP3 to PGE2: A rational target to prevent atherothrombosis without inducing bleeding. *Prostaglandins Other Lipid Mediat.* 2015;121(Pt A):4-16.

18.   Honda T, Matsuoka T, Ueta M, Kabashima K, Miyachi Y, and Narumiya S. Prostaglandin E(2)-EP(3) signaling suppresses skin inflammation in murine contact hypersensitivity. *J Allergy Clin Immunol.* 2009;124(4):809-18 e2.

19.   Amano H, Ito Y, Suzuki T, Kato S, Matsui Y, Ogawa F, et al. Roles of a prostaglandin E-type receptor, EP3, in upregulation of matrix metalloproteinase-9 and vascular endothelial growth factor during enhancement of tumor metastasis. *Cancer Sci.* 2009;100(12):2318-24.

20. Wang SZ, Dulin J, Wu H, Hurlock E, Lee SE, Jansson K, et al. An oligodendrocyte-specific zinc-finger transcription regulator cooperates with Olig2 to promote oligodendrocyte differentiation. *Development.* 2006;133(17):3389-98.

21. Biswas S, Chung SH, Jiang P, Dehghan S, and Deng W. Development of glial restricted human neural stem cells for oligodendrocyte differentiation in vitro and in vivo. *Sci Rep.* 2019;9(1):9013.

22. Ogawa F, Amano H, Eshima K, Ito Y, Matsui Y, Hosono K, et al. Prostanoid induces premetastatic niche in regional lymph nodes. *J Clin Invest.* 2014;124(11):4882-94.

23. Kashiwagi E, Shiota M, Yokomizo A, Itsumi M, Inokuchi J, Uchiumi T, et al. Prostaglandin receptor EP3 mediates growth inhibitory effect of aspirin through androgen receptor and contributes to castration resistance in prostate cancer cells. *Endocr Relat Cancer.* 2013;20(3):431-41.

24. Zong D, Jiang N, Xu JH, Wang DJ, Zhu HF, Wu LR, et al. ZNF488 is an independent prognostic indicator in nasopharyngeal carcinoma and promotes cell adhesion and proliferation via collagen IV/FAK/AKT/Cyclin D1 pathway. *Cancer Manag Res.* 2019;11:5871-82.

25. Zhang X, Li L, Liu P, Tian Y, and Gong P. Development of a Transcription Factor-Based Prognostic Model for Predicting the Immune Status and Outcome in Pancreatic Adenocarcinoma. *J Immunol Res.* 2022;2022:4946020.

26. Chen D, Le SB, Hutchinson TE, Calinescu AA, Sebastian M, Jin D, et al. Tumor Treating Fields dually activate STING and AIM2 inflammasomes to induce adjuvant immunity in glioblastoma. *J Clin Invest.* 2022;132(8).

27. Hoang-Minh LB, Siebzehnrubl FA, Yang C, Suzuki-Hatano S, Dajac K, Loche T, et al. Infiltrative and drug-resistant slow-cycling cells support metabolic heterogeneity in glioblastoma. *The EMBO Journal.* 2018;37(23):e98772.

28. Allen M, Bjerke M, Edlund H, Nelander S, and Westermark B. Origin of the U87MG glioma cell line: Good news and bad news. *Science Translational Medicine.* 2016;8(354):354re3-re3.

29. Hu Y, and Smyth GK. ELDA: Extreme limiting dilution analysis for comparing depleted and enriched populations in stem cell and other assays. *Journal of Immunological Methods.* 2009;347(1):70-8.

30. Diamant G, Simchony Goldman H, Gasri Plotnitsky L, Roitman M, Shiloach T, Globerson-Levin A, et al. T Cells Retain Pivotal Antitumoral Functions under Tumor-Treating Electric Fields. *J Immunol.* 2021;207(2):709-19.

31. Breznik B, Motaln H, Vittori M, Rotter A, and Lah Turnšek T. Mesenchymal stem cells differentially affect the invasion of distinct glioblastoma cell lines. *Oncotarget.* 2017;8(15):25482-99.

32. Ishii N, Maier D, Merlo A, Tada M, Sawamura Y, Diserens AC, et al. Frequent co-alterations of TP53, p16/CDKN2A, p14ARF, PTEN tumor suppressor genes in human glioma cell lines. *Brain Pathol.* 1999;9(3):469-79.

33. Verhaak RG, Hoadley KA, Purdom E, Wang V, Qi Y, Wilkerson MD, et al. Integrated genomic analysis identifies clinically relevant subtypes of glioblastoma characterized by abnormalities in PDGFRA, IDH1, EGFR, and NF1. *Cancer Cell.* 2010;17(1):98-110.

34. Liu T, Jin D, Le SB, Chen D, Sebastian M, Riva A, et al. Machine Learning-Directed Conversion of Glioblastoma Cells to Dendritic Cell-like Antigen-Presenting Cells as Cancer Immunotherapy. *Cancer Immunol Res.* 2024.

35. Consortium GO. The Gene Ontology resource: enriching a GOld mine. *Nucleic Acids Res.* 2021;49(D1):D325-d34.

36. Singh, Hawkins, Clarke, Squire, Bayani, Hide, et al. Identification of human brain tumour initiating cells. *Nature.* 2004;432(7015):396-401.

37. Prager BC, Bhargava S, Mahadev V, Hubert CG, and Rich JN. Glioblastoma Stem Cells: Driving Resilience through Chaos. *Trends Cancer.* 2020;6(3):223-35.

38. Dey I, Lejeune M, and Chadee K. Prostaglandin E2 receptor distribution and function in the gastrointestinal tract. *Br J Pharmacol.* 2006;149(6):611-23.

39. Lathia JD, Mack SC, Mulkearns-Hubert EE, Valentim CL, and Rich JN. Cancer stem cells in glioblastoma. *Genes Dev.* 2015;29(12):1203-17.

40. Vassalli G. Aldehyde Dehydrogenases: Not Just Markers, but Functional Regulators of Stem Cells. *Stem Cells Int.* 2019;2019:3904645.

41. Singh SK, Hawkins C, Clarke ID, Squire JA, Bayani J, Hide T, et al. Identification of human brain tumour initiating cells. *Nature.* 2004;432(7015):396-401.

42. Soundarapandian MM, Selvaraj V, Lo UG, Golub MS, Feldman DH, Pleasure DE, et al. Zfp488 promotes oligodendrocyte differentiation of neural progenitor cells in adult mice after demyelination. *Sci Rep.* 2011;1:2.

43. Dittmer TA, and Misteli T. The lamin protein family. *Genome Biology.* 2011;12(5):222.

44. Suno R, Sugita Y, Morimoto K, Takazaki H, Tsujimoto H, Hirose M, et al. Structural insights into the G protein selectivity revealed by the human EP3-Gi signaling complex. *Cell Reports.* 2022;40(11):111323.

45. Kim SO, Dozier BL, Kerry JA, and Duffy DM. EP3 receptor isoforms are differentially expressed in subpopulations of primate granulosa cells and couple to unique G-proteins. *Reproduction.* 2013;146(6):625-35.

46. Namba T, Sugimoto Y, Negishi M, Irie A, Ushikubi F, Kakizuka A, et al. Alternative splicing of C-terminal tail of prostaglandin E receptor subtype EP3 determines G-protein specificity. *Nature.* 1993;365(6442):166-70.

47. Wang S-Z, Dulin J, Wu H, Hurlock E, Lee S-E, Jansson K, et al. An oligodendrocyte-specific zinc-finger transcription regulator cooperates with Olig2 to promote oligodendrocyte differentiation. *Development.* 2006;133(17):3389-98.

48. Bhattacharya M, Peri K, Ribeiro-da-Silva A, Almazan G, Shichi H, Hou X, et al. Localization of functional prostaglandin E2 receptors EP3 and EP4 in the nuclear envelope. *J Biol Chem.* 1999;274(22):15719-24.

49.   Bhattacharya M, Peri KG, Almazan G, Ribeiro-da-Silva A, Shichi H, Durocher Y, et al. Nuclear localization of prostaglandin E2 receptors. *Proc Natl Acad Sci U S A.* 1998;95(26):15792-7.

50.   Hasegawa H, Katoh H, Yamaguchi Y, Nakamura K, Futakawa S, and Negishi M. Different membrane targeting of prostaglandin EP3 receptor isoforms dependent on their carboxy-terminal tail structures. *FEBS Lett.* 2000;473(1):76-80.

51.   Lytle NK, Barber AG, and Reya T. Stem cell fate in cancer growth, progression and therapy resistance. *Nature Reviews Cancer.* 2018;18(11):669-80.

52.   Dean M, Fojo T, and Bates S. Tumour stem cells and drug resistance. *Nature Reviews Cancer.* 2005;5(4):275-84.

53.   Mawhin M-A, Tilly P, and Fabre J-E. The receptor EP3 to PGE2: A rational target to prevent atherothrombosis without inducing bleeding. *Prostaglandins & Other Lipid Mediators.* 2015;121:4-16.

54.   Tilly P, Charles A-L, Ludwig S, Slimani F, Gross S, Meilhac O, et al. Blocking the EP3 receptor for PGE2 with DG-041 decreases thrombosis without impairing haemostatic competence. *Cardiovascular research.* 2014;101(3):482-91.

Figure legends

Figure 1: EP3 is the predicted master regulator of TTFields resistance in GBM.

A) A schema detailing the experimental protocol to generate TTFields-resistant GBM cells and determine the temporal development of TTFields resistance.

B) Line plots of the growth rates of the 3 indicated GBM cell lines treated with TTFields continuously for 7 (TTF7D), then 14 (TTF14D), 21 (TTF21D), 28 (TTF28D), and 35 (TTF35D) days, showing that resistant cells emerged by TTF21D.

C) An expression heatmap of the 3 GBM cell lines treated with continuous TTFields, showing that expression changes in TTFields-resistant TTF28-35D cells were also observed in TTF7D cells — well before the emergence of resistance.

D-E) 3D maps of changes in regulatory hubs in the 3 GBM cell lines in indicated treatment periods as TTFields resistance develops. Red — upregulation; Blue — downregulation; Grey — unchanged; Globe size — number of pathways in a hub.

F) A line plot of a time course of EP3 mRNA levels in the 3 GBM cell lines treated with continuous TTFields.

G) EP3 expression in the 3 TTFields-resistant (R) GBM cell lines and their non-treated sensitive counterparts by immunoblotting (blot image) and quantified by densitometry relative to β-actin (bar graph).

H) Bar plots of the sphere numbers per 1000 GSC (left) and mean sphere size (right) after 3-day TTFields treatment (TTF3D) in the 3 TTFields-resistant (R) GSC lines and their non-treated

42

sensitive counterparts. Resistant cells were first generated after 35 days of continuous TTFields treatment.

I) A 2D map of a 500-top ranked gene regulatory network in TTFields-resistant GSC compared to their non-treated sensitive counterparts, showing EP3 occupy a prominent position with numerous links to the 3 hallmark functional hubs of GSC. Node color — expression logFC per heatmap scale.

J-K) EP3 expression in the 3 TTFields-resistant (R) GSC lines and their non-treated sensitive counterparts as determined by qRT-PCR (**J**) and immunoblotting (blot images) and quantified by densitometry relative to β-actin (bar graph) (**K**).

All experiments in triplicate were repeated at least 3 times. Data are represented as mean ± SEM. ANOVA test was used for **B** and **I** and Student's t-test with a 2-tailed distribution for **H** and **J-K**. *, $P <0.05$; **, $P <0.01$; ***, $P <0.001$; ns: not significant.

Figure 2: EP3 inhibition and overexpression reverses and induces TTFields resistance, respectively, in GSC.

A) A diagram depicting the arachidonic acid pathway. EP3 has the highest affinity for PGE2, and the only receptor coupled with Gαi, which reduces cAMP levels.

B-E) Bar plots of the remaining sphere number per 1000 GSC (top) and mean sphere size (bottom) of the 3 TTFields-resistant GSC lines after 3-day TTFields treatment (TTF3D) concurrent with aspirin (0.5mM) (**B**), DG041 (50nM) (**C**), L798,106 (L798, 500nM) (**D**) or the vehicle, or one of the 2 independent *shEP3* shRNA or the *shScrambled* (*shScr*) control (**E**).

F) Bar plots (top) showing that overexpression of EP3 — confirmed by immunoblotting (bottom) — in the 3 GSC lines specifically conferred TTFields resistance. Sphere number and size remaining after 3 days with or without TTFields are expressed as a percentage of the respective non-TTFields-treated (NT) control.

All experiments in triplicate were repeated at least 3 times. Data are represented as mean ± SEM. Student's t-test with a 2-tailed distribution was used for **B-D**, and ANOVA for **E-F**. *, P <0.05; **, P <0.01; ***, P <0.001; ns: not significant.

Figure 3: EP3 inhibition preemptively prevents development of TTFields resistance.

A) Line plots of the growth rates of the 3 GBM cell lines treated with continuous TTFields for indicated durations concurrent with 500nM L798,106 (L798) or the vehicle.

B) Bar plots of the sphere number per 1000 GSC (left) and mean sphere size (right) of the 3 GSC lines treated with continuous TTFields for 35 days (TTF35D) concurrent with 500nM L798,106 (L798) or the vehicle.

All experiments in triplicate were repeated at least 3 times. Data are represented as mean ± SEM. ANOVA was used for analysis. *, P <0.05; **, P <0.01; ***, P <0.001; ns: not significant.

Figure 4: EP3 inhibition reduces self-renewal and tumorigenicity of TTFields-resistant GSC.

A-B) Bar graphs of geometric means of expression of the GSC markers ALDH1A1 (**A**) and CD133 (**B**) in the 3 TTFields-resistant GSC lines and non-treated sensitive counterparts, expressing one of the 2 *shEP3* shRNA or *shScrambled* (*shScr*) control.

C-E) Combo box, whisker, and dot plots of the sphere number per 1000 GSC (left) and mean sphere size (right) of the 3 TTFields-resistant (R) GSC and their non-treated sensitive counterparts treated with 500nM L798,106 (L798) or vehicle and with or without 3-day TTFields treatment (TTF3D). Resistant cells were maintained under TTFields treatment.

F-H) Kaplan-Meier estimates showing survival rates after orthotopic implantation of the same GSC lines in **C-E** (10^4 cells for L2 and CA3 and 10^5 for CA7) into equal numbers of male and female 6-week-old NSG mice. Median survival (in days) is shown next to each group label; NR = median survival not reached. N=10 mice in each group.

All experiments in triplicate were repeated at least 3 times. Data are represented as mean ± SEM. For box and whisker plots, the whiskers are the minimum and maximum values, the lower and upper box edges the 25th and 75th percentage values, respectively, and the lines within the boxes the median. ANOVA was used for **A-E**, and log-rank for in **F-H**. *, $P <0.05$; **, $P <0.01$; ***, $P <0.001$; ns: not significant.

Figure 5: EP3 inhibition reduces self-renewal and tumorigenicity of GSC freshly isolated from TTFields-resistant tumors in response to TTFields.

A) The experimental schema to study EP3's role in self-renewal and tumorigenicity of GSC freshly isolated from TTFields-resistant tumors. GSC23 and GSC33 were positive and GSC122 negative for MGMT promoter methylation.

B) A bar graph of EP3 mRNA expression in the 3 freshly isolated GSC lines as compared to the other 3 TTFields-resistant GSC lines.

C-E) Combo box, whisker, and dot plots of the sphere number per 1000 GSC (left) and mean sphere size (right) of the 3 fresh GSC lines treated with 500nM L798,106 (L798) or the vehicle and with or without 3-day TTFields treatment (TTF3D).

F-H) Kaplan-Meier estimates showing survival rates after orthotopic implantation of the same GSC lines in **C-E** (10^4 cells of each freshly isolated GSC line) into equal numbers of male and female 6-week-old NSG mice. Median survival (in days) is shown next to each group label; NR = median survival not reached. N=10 mice in each group.

All experiments in triplicate were repeated at least 3 times. Data are represented as mean ± SEM. For box and whisker plots, the whiskers are the minimum and maximum values, the lower and upper box edges the 25th and 75th percentage values, respectively, and the lines within the boxes the median. ANOVA was used for **C-E**, and log-rank for **F-H**. *, $P < 0.05$; **, $P < 0.01$; ***, $P < 0.001$; ns: not significant.

Figure 6: ZNF488 is required for TTFields resistance in GBM cells.

A-D) 2D maps comparing EP3-associated and neighboring pathways in the 3 GBM cell lines in indicated treatment periods, showing ZNF488 is a co-master regulator of EP3 in the stemness hub by 7D (purple arow) and reinforced by 28–35D of TTFields exposure (broken circle).

E-F) ZNF488 is upregulated in the 3 TTFields-resistant GSC lines as measured in mRNA (**E**) and protein by immunoblotting quantified by densitometry relative to β-actin (**F**).

46

G) Bar graphs of the sphere numbers per 1000 GSC (top) and mean sphere size (bottom) after 3-day TTFields treatment (TTF3D) in the 3 TTFields-resistant (R) GSC lines and their non-treated sensitive counterparts, expressing *shZNF488-1* shRNA or *shScr*. Inset: ZNF488 protein depletion by the 2 *shZNF488* in L2-R and CA3-R.

H) A 2D map of the 1000-gene, ZNF488-regulated subnetwork with 3 hallmark GSC pathways.

I) Bar graphs of mRNA expression of key genes in the ZNF488-regulated subnetwork shown in (**H**) in the 3 GSC lines in response to ZNF488 depletion by *shZNF488-1* shRNA or *shScr* control.

All experiments in triplicate were repeated at least 3 times. Data are represented as mean ± SEM. In **A-D** and **H**: Node size — importance rank of a gene. Node color: Red — upregulation; Blue — downregulation; Grey — unchanged. Student's T-test with a 2-tailed distribution was used for **E-F** and **I**, and ANOVA for **G**. *, $P <0.05$; **, $P <0.01$; ***, $P <0.001$; ns: not significant.

Figure 7: EP3 binds ZNF488 in the nucleus in resistant cells.

A) Confocal images with Z stack showing colocalization of EP3 and LaminAC (yellow) in LN827 cells following 24-hr treatment with TTFields. Representatives of 3 independent experiments are shown. Scale bar = 10μm; Z-heigh = 15μm.

B-C) EP3 and ZNF488 are co-localized in the nucleus in TTFields-resistant (R) cells, as shown by IF for EP3, ZNF488, and LaminAC with DAPI counter-staining in LN827-R cells (**B**), and by subcellular fractionation in LN827-R and the GSC L2-R and CA3-R lines (**C**) as compared to

their non-treated sensitive counterparts. Representatives of 3 independent experiments are shown. Scale bar = 10μm in **B**.

D) Immunoblot images showing ZNF488 is specifically co-immunoprecipitated (co-IP) with EP3 in TTFields-resistant LN827-R (top), L2-R (middle), and CA3-R (bottom).

E) Diagrams of the domains of EP3 (top) and ZNF488 (bottom). Full length and truncated mutants of EP3 were created with a N-terminal 6xHis tag and those of ZNF488 with a C-terminal Flag tag.

F) Immunoblot images of relative co-IP efficiency of (Top) 6xHis-tagged full-length EP3 (FL-EP3) or its truncated mutants — EP3-N (without N-terminal domain), EP3-IL2 (without IL2 domain), and EP3-C (without C-terminal domain) — and (bottom) Flag-tagged full-length ZNF488 (FL-ZNF488) or its truncated mutants — ZNF-RD (without repression domain) and ZNF-ZF (without Zn finger domain) — as compared to the IgG1 isotype control in HEK 293 cells.

G) Bar graphs of the sphere number per 1000 GSC (top) and mean sphere size (bottom) after 24-hr TTFields treatment in L2 GSC expressing either the empty virus (ev) or one of the indicated combinations of full-length and truncated mutants of EP3 and ZNF488.

H) Relative co-IP efficiency of FL-EP3 (6xHis) and FL-ZNF488 (Flag) in L2 GSC treated with increasing concentrations of L798,106 (L798) using anti-His antibody or the IgG1 isotype control for IP and anti-EP3 and anti-Flag for IB (top immunoblot images) and quantified by densitometry of co-precipitated ZNF488 (Flag) levels relative to input and normalized to the Vehicle control (bottom bar graph).

Data are represented as mean ± SEM. ANOVA was used for **G-H**. *, $P < 0.05$; **, $P < 0.01$; ***, $P < 0.001$; ns: not significant.

Figure 8: Epistatic interaction between EP3 and ZNF488 in TTFields resistance.

A) Combo box, whisker, and dot plots of the sphere number per 1000 GSC (top) and mean sphere size (bottom) of the 3 GSC lines treated with 3-day TTFields (TTF3D) or non-treated (NT), while overexpressing either EP3 with or without *shZNF488-1* or ZNF488 with or without *shEP3-1*, following 3D TTFields treatment (TTF).

B-C) Combo box, whisker, and dot plots of EP3 (**B**) and ZNF488 (**C**) mRNA expression by bulk RNA-seq of paired primary and recurrent GBM tumors from patients treated with TMZ alone (left; n = 6) or TMZ plus TTFields (right; n = 7).

D) Bar graphs of EP3 (left) and ZNF488 (right) mRNA in indicated cancer lines before (NT) and after 24-hr 150-kHz TTFields treatment (TTF1D). T24 and UMUC3 are human bladder epithelial carcinoma; MDA-MB-231 human triple negative breast carcinoma; HeLa human cervical carcinoma; PANC-1 human pancreatic ductal adenocarcinoma; A549 human lung adenocarcinoma; 786-O human renal cell carcinoma; and B16 murine melanoma.
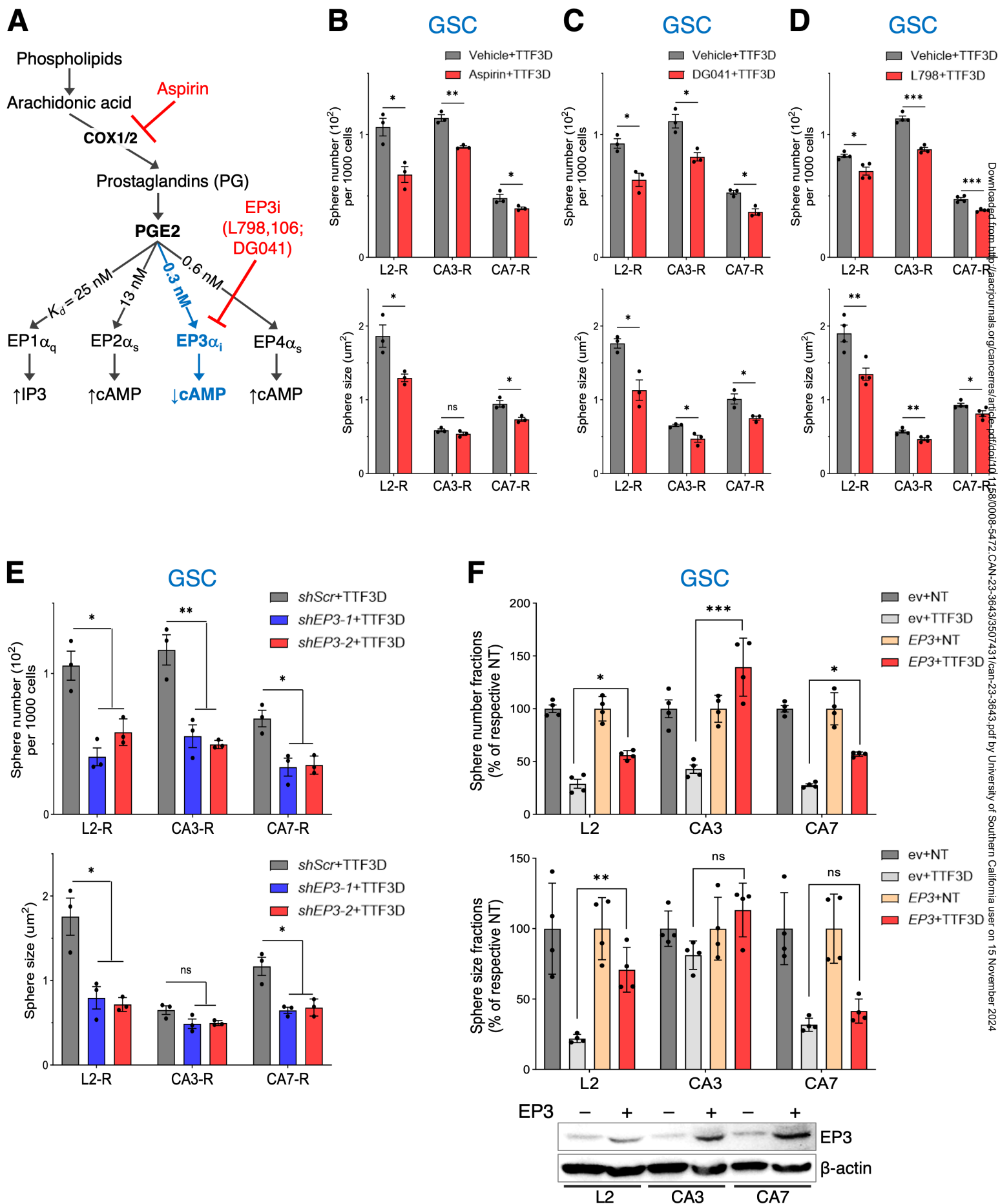
E) Kaplan-Meier estimates showing survival rates in patients with indicated cancers in TCGA with high ($EP3^{hi}$; $ZNF488^{hi}$) or low ($EP3^{lo}$; $ZNF488^{lo}$) co-expression of EP3 and ZNF488, defined by above or below median expression of each protein, respectively. SKCM — Skin/melanoma; KIRP — renal papillary cancer; PAAD — pancreatic ductal carcinoma; UCEC — uterine carcinoma; and BLCA — bladder epithelial carcinoma.

49

All experiments in triplicate were repeated at least 3 times. Data are represented as mean ± SEM. For box and whisker plots, the whiskers are the minimum and maximum values, the lower and upper box edges the 25th and 75th percentage values, respectively, and the lines within the boxes the median. ANOVA was used for **A**, paired Student's T-test for **B-C**, Student's T-test with a 2-tailed distribution for **D**, and log-rank for **E**. *, $P <0.05$; **, $P <0.01$; ***, $P <0.001$; ns: not significant.
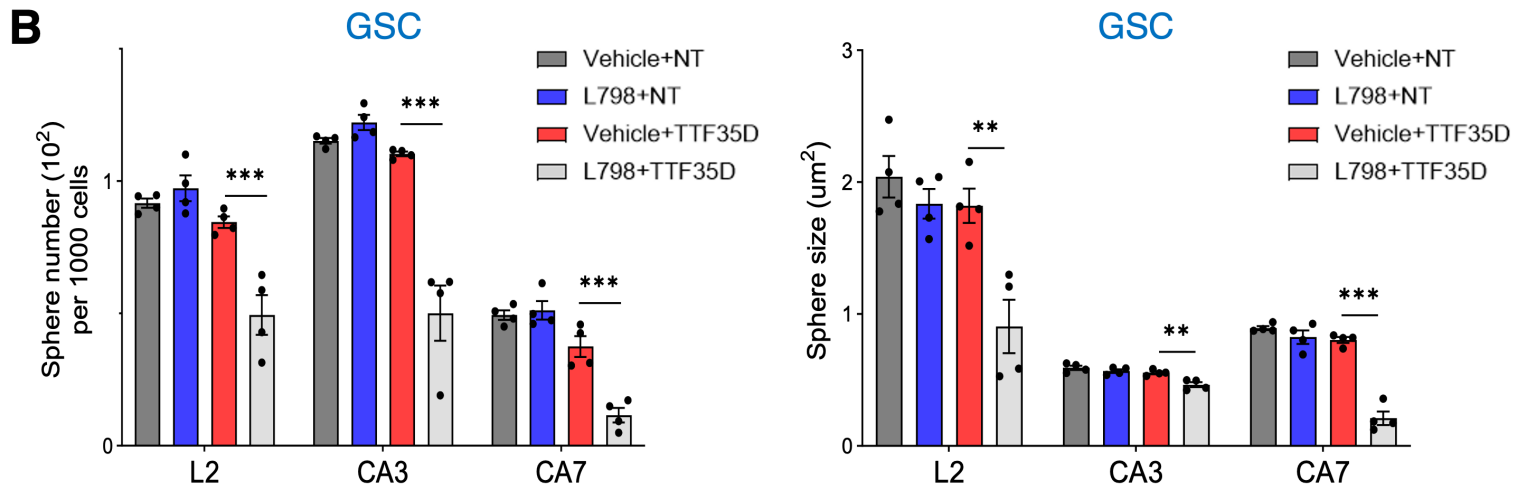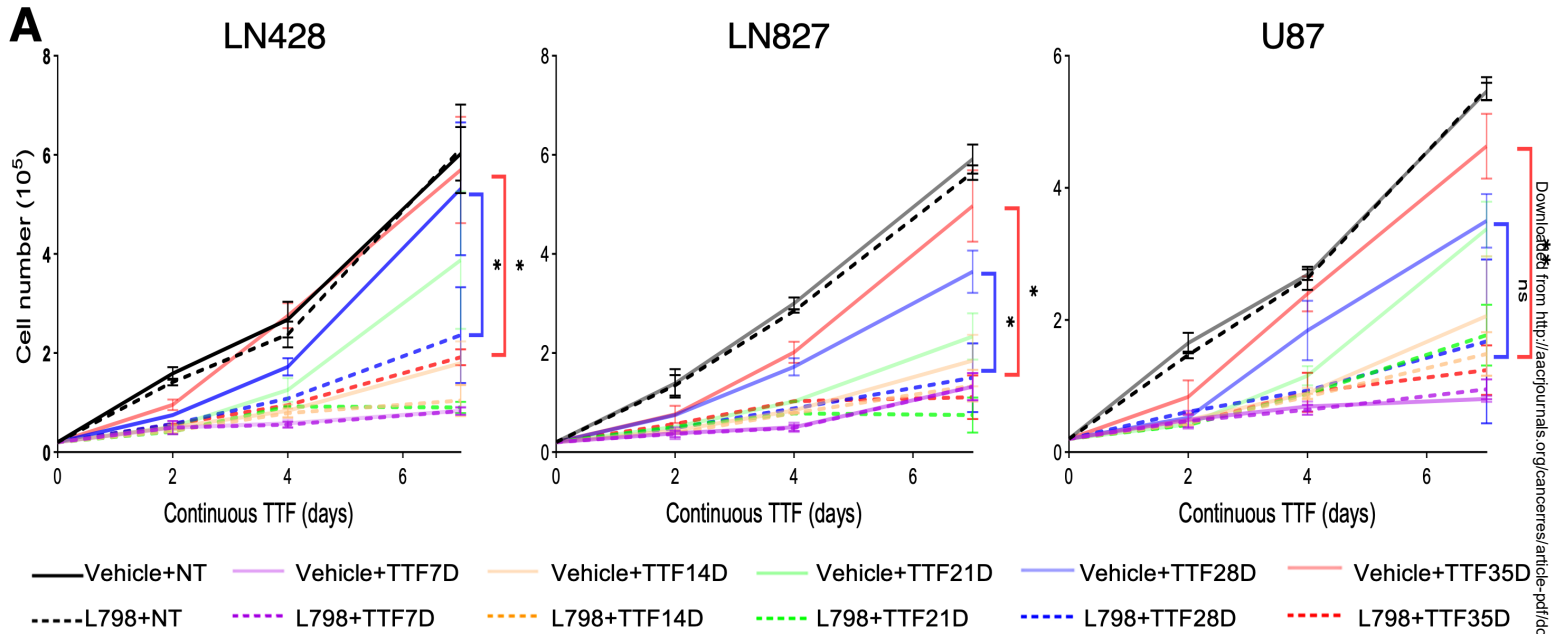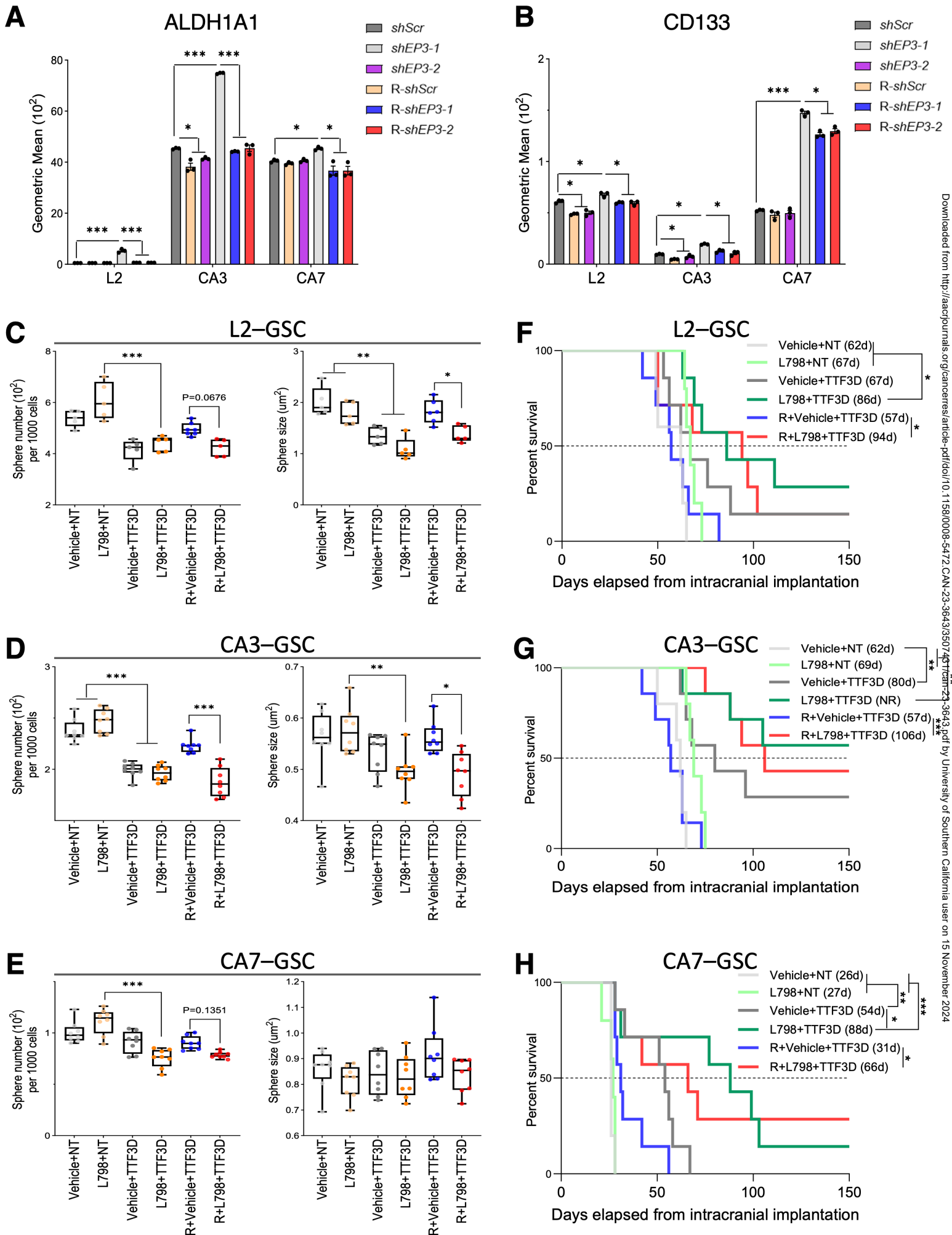
Figure 1

Figure 2

Figure 3

A

LN428 / LN827 / U87: Cell number (10^5) vs Continuous TTF (days)

Legend:
— Vehicle+NT — Vehicle+TTF7D — Vehicle+TTF14D — Vehicle+TTF21D — Vehicle+TTF28D — Vehicle+TTF35D
--- L798+NT --- L798+TTF7D --- L798+TTF14D --- L798+TTF21D --- L798+TTF28D --- L798+TTF35D

B

GSC: Sphere number (10^2) per 1000 cells — L2, CA3, CA7

GSC: Sphere size (μm^2) — L2, CA3, CA7

Legend:
- Vehicle+NT
- L798+NT
- Vehicle+TTF35D
- L798+TTF35D
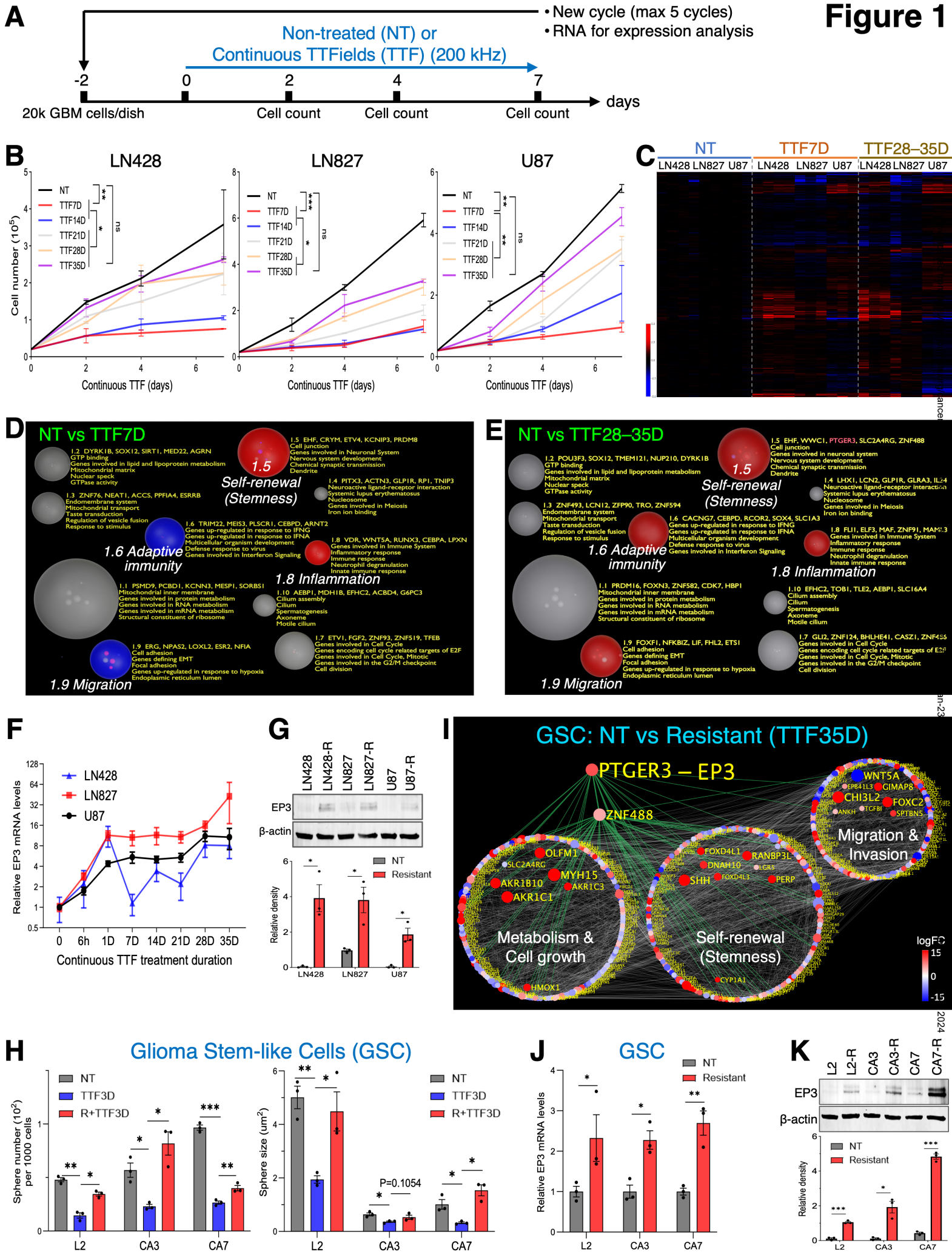
Figure 4

Figure 5

Figure 6

A NT vs TTF1D

B NT vs TTF7D

C NT vs TTF28–35D

D TTF7D vs TTF28–35D

E GSC

F GSC

G GSC

H PTGER3 – EP3

I L2-R, CA7-R, CA3-R GSC

Figure 7

Figure 8